

Asymmetric magnetization reversal of the Heusler Alloy Co_2FeSi as Free Layer in an $\text{CoFeB}/\text{MgO}/\text{Co}_2\text{FeSi}$ Magnetic Tunnel Junction

Yury P. Kabanov,^{1,2} Robert D. Shull,¹ Chao Zheng,³ Philip W. T. Pong,³ and Daniel B. Gopman^{1*}

1. Materials Science and Engineering Division, National Institute of Standards and Technology, Gaithersburg, MD, 20899, USA
2. Institute for Solid Physics, Russian Academy of Sciences, Chernogolovka 142432, Russia
3. Department of Electrical and Electronic Engineering, University of Hong Kong, Hong Kong

KEYWORDS: magnetic domain imaging; MRAM; Co_2FeSi ; heusler alloy

Abstract:

We report the in-plane magnetization reversal behavior of the Co_2FeSi Heusler alloy free layer in a bottom-pinned magnetic tunnel junction film with 149% TMR. Using magneto-optic indicator film imaging, we visualize the magnetic domain dynamics of this buried layer integrated within a full magnetic tunnel junction stack. The magnetic domain dynamics reveal anisotropic magnetization reversal within Co_2FeSi under applied in-plane magnetic fields. While the reversal behavior under in-plane fields applied perpendicular to the in-plane exchange bias direction indicates smooth, coherent rotation away from the easy axis, asymmetric magnetic reversal behavior is observed along the easy axis. Reversed domains propagate from the interior of the film laterally outward toward the edges as the free layer magnetization switches into parallel alignment with the pinned synthetic antiferromagnetic reference layer ($\text{IrMn}/\text{CoFe}/\text{Ru}/\text{CoFeB}$). On the other hand, domains propagate from the film edges inward for the free layer transition into antiparallel alignment with the reference layer. These results have important implications for Heusler magnetic tunnel junction device performance.

*Corresponding author: daniel.gopman@nist.gov

1. Introduction

Magnetic tunnel junctions with MgO tunneling barriers have a significant technological footprint in magnetic field sensing and non-volatile magnetic memory applications. Achieving ever larger tunneling magnetoresistance (TMR) values plays a significant role in advancing the overall sensitivity of magnetic field sensors and the ON/OFF ratio of memory cells. To this end, successful realizations of high TMR values have been realized using various CoFe and CoFeB alloys, which have fully spin-polarized Δ_1 and Bloch states at the Fermi level and take advantage of coherent tunneling through the MgO tunneling barrier. Heusler alloys have also been considered as candidates for the ferromagnetic electrodes spanning the MgO tunneling barrier due to their half-metallic ferromagnetic behavior which leads to relatively high spin polarization at room temperature. Significantly high TMR values have been realized in several Heusler-based MTJs, including a high TMR values at room temperature of 217% in a CoFe/MgO/Co₂MnSi stack [1], 180% by E. Ozawa in a Co₂MnAl/MgO/CoFe stack [2], 340% by W. Wang in a Co₂FeAl/MgO/CoFeAl/CoFe stack structure [3], and 386% in stacks of Co₂FeAl_{0.5}Si_{0.5}/MgO/Co₂FeAl_{0.5}Si_{0.5}/CoFe [4].

The full Heusler material Co₂FeSi has drawn significant attention due to its promise for highly spin polarized transport, combined with particularly large saturation magnetization ($6 \mu_B$) and a high Curie Temperature (1100 K) amongst Heusler alloys [5]. L₂₁ ordered Co₂FeSi films exhibit desirable properties for integration into magnetic sensor and memory devices, including a modest magnetic anisotropy, high exchange stiffness and low Gilbert damping [6]. Magneto-optic studies have shown unusually large quadratic magneto-optic effects, indicating unusually large high-order spin-orbit coupling effects [7]. A photoemission electron microscopy with x-ray magnetic circular dichroism study of a polycrystalline Co₂FeSi bulk specimen has shown low anisotropy and strain-induced magnetic ripple domain patterns [8].

While many of the previous studies investigated Heusler alloys grown on single-crystalline MgO(001) substrates, we have demonstrated the possibility of integration with silicon-based microelectronics by using thermally oxidized silicon substrates to grow full Heusler (e.g. Heusler/MgO/Heusler) and mixed CoFeB-Heusler (e.g. CoFeB/MgO/Heusler or Heusler/MgO/CoFeB) MTJs [9]. The behavior of Co₂FeSi as a free layer (FL) integrated into an MTJ must be understood to determine whether its advantageous material properties translate into device performance.

This letter explores the reversal behavior of a Co₂FeSi integrated as the FL an in-plane magnetized MTJ grown on thermally oxidized silicon. The magneto-optic indicator film (MOIF) technique is used to image magnetic domains in the Co₂FeSi free layer (FL) during reversal under in-plane fields applied parallel or perpendicular to the exchange biased reference layer (RL). Unlike surface characterization techniques such as scanning electron microscopy with polarization analysis and magneto-optic Kerr effect imaging, the MOIF technique enables non-destructive, *in operando* magnetic domain observations of the Co₂FeSi layer, with sensitivity to the microscopic magnetization configurations within this layer despite being buried under thick metal capping electrodes. For fields applied in-plane and perpendicular to the exchange bias, the Co₂FeSi layer magnetization rotates coherently toward the direction of applied field, exhibiting soft magnetic

properties desirable for magnetic sensing. On the other hand, fields applied parallel to the RL leads to anisotropic domain propagation. The reversed domains nucleate at the sample edge for parallel alignment of the Co_2FeSi with the RL magnetization and alternatively nucleate from within the interior during the parallel to anti-parallel FL transition. These magnetic domain observations at lateral sizes of order $10\ \mu\text{m}$ yields insight into the behavior of this technologically promising structure at the mesoscale, bridging the macroscopic details closer to the more device relevant sub- μm length scales.

2. Material and methods

The sample was grown on a thermally oxidized silicon substrate using magnetron sputtering at room temperature in an ultrahigh vacuum chamber with a base pressure of 6.6×10^{-7} Pa. An argon pressure of 0.24 Pa was maintained during sputter deposition of the layers. The sample structure was as follows: Substrate/Ta(5 nm)/IrMn(7.5 nm)/CoFe(4 nm)/Ru(0.8 nm)/ $\text{Co}_{20}\text{Fe}_{60}\text{B}_{20}$ (3.5 nm)/MgO(2 nm)/ Co_2FeSi (4 nm)/Ta(5 nm)/Ru(10 nm). The MgO tunnel barrier was deposited under radio frequency power while the other layers were deposited using direct current power. The Co_2FeSi layer was grown by simultaneous sputtering from pure Co, Fe and Si targets. All other layers were grown by sputtering from single element or stoichiometric alloy targets. The film was post-annealed in vacuum at 360 C for 1 h under a 0.5 T in-plane field to enhance the TMR and to set the exchange bias direction of the CoFe/Ru/CoFeB synthetic antiferromagnetic reference layer.

Current-in-plane tunneling (CIPT) measurements of the sample was carried out using a CAPRES CIPT Tester to evaluate the top (R_t) and bottom (R_b) sheet resistances, resistance-area (RA) product of the tunnel barrier and the TMR ratio. Figure 1 shows the resistance and CIPT MR versus probe spacing averaged over several representative regions over a 25 mm square specimen. Error bars reflect the one-sigma variance of measured resistance (CIPT MR) values. The estimated parameters of this MTJ that best fit the CIPT model [10] are $R_t = 16.9(2)\ \Omega$, $R_b = 6.5(3)\ \Omega$, $RA = 1100(80)\ \Omega\cdot\mu\text{m}^2$ and $\text{TMR} = 149(1)\ \%$. The high TMR value is comparable to other in-plane magnetized MTJs that incorporate other Heusler materials into the free layer.

Magneto-optic imaging of the reversal behavior of the free layer was carried out at room temperature and under applied magnetic fields oriented along the easy and hard axes of the MTJ. Imaging of the magnetization was achieved by the magneto-optical indicator film (MOIF) technique [11, 12]. This technique utilizes the high Faraday rotation and the in-plane anisotropy of a Bi-substituted garnet indicator film – on a transparent garnet substrate - placed directly on top of the MTJ film. The magneto-optic contrast is formed by local changes in the Faraday rotation of the MOIF film. The MOIF film produces an image from the stray fields of the underlying sample emerging from edges or domain walls, enabling real time domain imaging of the specimen [13-15]. This technique has been particularly useful for real-time magnetic domain imaging of both surfaces and buried layers, and particularly of coupled layers in magnetic multilayers and spin valve structures [16-18]. For an in-plane magnetized MTJ film, out-of-plane fields are generated exclusively at discontinuities in the magnetic texture, either at a sample edge or across a domain wall. The presence of a hole in a sample can be used to estimate the average magnetization angle of the surrounding region [16]. The magnetostatic field on each side of the hole collinear with the background sample magnetization is equal and opposite, casting a region of white and black MO

contrast on the opposite sides of the hole due to the opposing Faraday rotation angles. Advantageously, this sample exhibits a circular hole in the thin film deposit along the sample edge enabling the observation of the magnetization rotation during reversal.

3. Results and Discussion

Magnetization versus applied field hysteresis loops were obtained using vibrating sample magnetometry under in-plane fields parallel and perpendicular to the in-plane exchange bias direction. Figure 2 highlights the low-field range around which the magnetization reversal of the Co_2FeSi layer occurs. Under fields applied along the exchange bias direction, the free layer hysteresis loop has a coercive field of approximately 1 mT and is offset from zero by -1.5 mT due to coupling with the reference layer. The inset shows an expanded field region that also includes the remagnetization of the SAF reference layer at high fields. For an in-plane field applied perpendicular to the exchange bias direction, the free layer shows a hard axis remagnetization behavior, with a saturation field near 7 mT.

Figure 3 presents the remagnetization process under in-plane applied magnetic fields along the vertical (hard) axis and perpendicular to the in-plane exchange bias direction. Here the MOIF film is situated at the leftmost edge of the MTJ sample, where a nearly circular hole has been physically removed from the perimeter. The magnetization orientation is graphically depicted by the compass overlaid on each subfigure in Figure 3, in which the white end of the compass depicts the direction the magnetization vector is pointing. Consistent with the modest anisotropy field extracted from the free layer M vs H magnetization curves in Figure 2, the magnetization is fully rotated into the positive vertical direction under a 6.9 mT applied magnetic field, as can be seen by the bright and dark contrast on opposite sides of the circular edge in Figure 3(a). As the field is reduced through zero to a negative saturating field of -6.9 mT (Figure 3), the magnetization rotates clockwise from up to down. This is mostly consistent with the extremely low hysteresis in the M vs H magnetization curves along the hard axis and a description of 180° coherent rotation under hard axis fields. Upon closer inspection, domain walls are observed in Figure 3, nucleating from the perimeter of the hole and annihilating on the sample edge and vice versa when returning the field to 6.9 mT. Magnetic domains walls do not spontaneously appear within the free layer far from the edge, which may explain the absence of a measurable coercivity in the hard axis hysteresis loop.

Subsequent frames depict the remagnetization behavior as the magnetic field is swept from a modest negative value to a modest positive value along the increasing branch of the hysteresis loop. The reversal dynamic can similarly be described as a combination of predominantly rotation as the magnetic field cycles from -3.5 mT to -0.7 mT in Figure 3 and a lesser contribution from magnetic domain wall propagation nearby the top- and bottom edges of the hole. The down-to-up magnetization rotation under positive fields exhibits a preferred counter-clockwise rotation, in contrast to the up-to-down magnetization process under negative fields. Moreover, despite the near-zero remanent magnetization along the vertical axis, a preferred magnetization direction is evident along the horizontal positive direction after reducing the vertical field to zero from both positive and negative values (Figure 3).

The anisotropy in the preferred sense of magnetization rotation requires a broken in-plane symmetry in order to generate a well-defined chirality. This apparent chirality shares similarities with rotational hysteresis phenomena seen in exchange-biased systems [16, 19]. Furthermore, as with exchange-biased bilayers, this sample shows a unidirectional anisotropy, such that the magnetization prefers to lie along the positive horizontal direction in zero applied field, regardless of applied field history. While the free layer does not experience an exchange bias, it nevertheless experiences some uncompensated magnetostatic field from the synthetic antiferromagnetic reference field. Furthermore, interfacial roughness at the CoFeB/MgO/Co₂FeSi heterojunction interfaces can induce an orange-peel type coupling between the layers that provides an effective interlayer exchange [20, 21]. In this manner, the free layer still experiences a unidirectional anisotropy generated by the exchange biased reference layer through magnetostatic coupling. Although the magnitude of the unidirectional anisotropy field is much smaller than the exchange bias anisotropy field experienced by the reference layer, the free layer is sufficiently soft as to demonstrate significantly modified magnetization behavior, which is observed in the MOIF images.

The influence of magnetostatic coupling between the layers is also evident in the magnetization reversal under fields applied along the horizontal (easy) axis, collinear with the exchange bias. Magneto-optic images of the easy axis remagnetization behavior are shown in Figure 4. After the applied field is increased from -6.9 mT, magnetic domain walls propagate away from the sample edges and into the bulk at small negative fields (Figure 4). By zero field, the magnetization has changed direction 180°, evidenced by the dark-to-bright change in edge contrast from Figure 4 to Figure 4. The M vs H curve indicates that this corresponds to an anti-parallel alignment of the free and pinned layers, also minimizing magnetostatic energy. Minor changes in the contrast appear in the MOIF images under positive applied fields (Figure 4) as the free layer is already saturated along the direction of applied field.

Figure 4 shows that as the field is reduced back to negative saturation, the free layer initiates reversal at -1.3 mT. This transition to a parallel configuration of the two layers is associated with magnetic domain walls propagating from within the interior to the edge of the film. Figure 4 show the rotation of an elongated domain wall (dark contrast) as it approaches the sample edge. Here the domain boundary gradually wraps around the round perimeter as the small, oppositely magnetized region is pushed outward to the edge where it is ultimately reversed. The asymmetric domain nucleation and propagation regions in the free layer is correlated with the relative orientation of the magnetostatically-coupled layers due to dipolar fields, an effect that has been seen in coupled magnetic multilayered films and patterned devices [17, 18, 22, 23]. In this structure with a soft free layer ($\mu_0 H_C < 1.5$ mT), the local nucleation of reversed domains is followed by domain wall propagation. The local nucleation is determined partially by external factors including the magnetostatic energy between the free and pinned layers. Reversal of the free layer into an energetically favorable anti-parallel alignment with the pinned layer is assisted by the magnetostatic coupling field between the layers, which is maximum near the sample perimeter, depicted in the snapshot of domain boundaries moving away from the edge in Figure 4. During the transition into a parallel configuration, nucleation occurs in the film interior, where the

magnetostatic energy cost is considerably less than at the boundaries. This is followed by domain wall propagation toward the edges, shown in Figure 4.

The microscopic mechanisms of magnetization reversal in the MTJ sensor film shown here reflects the significant influence of the FL environment in a full MTJ on determining the reversal character. The magnetostatic coupling between the FL and RL remains the primary obstacle for engineering a soft, highly responsive Co₂FeSi-based MTJ. First, we demonstrated that edge effects can compete with the uniaxial and unidirectional anisotropies to generate both domain nucleation and rotation in the hard axis reversal mechanism. This could negatively influence the ability of patterned MTJ sensors to operate in a rotation-only mode, in which spurious domain wall nucleation from an edge could worsen the noise character of the sensor. Second, we show that the magnetostatic coupling imprints a fixed chirality on the free layer rotation during the hard axis reversal. Finally, for fields applied along the easy axis, we demonstrated the asymmetric nucleation of reversed domains relative to the orientation of the free and pinned layers. The reversal onto the direction of the pinned layer is initiated by nucleation in the sample interior where the magnetostatic coupling between the layers is lowest. On the other hand, magnetostatic coupling would appear to assist the magnetization of the free layer into an anti-parallel alignment with the fixed layer, supported by our MO observations of edge nucleation followed by domain wall propagation into the sample interior. While the magnetostatic coupling field in these samples appears small according to the hysteresis loop shift (-0.6 mT), patterned MTJ sensors will exhibit significantly larger magnetostatic coupling fields. The somewhat deleterious attributes observed in this particular MTJ are not likely to lead to fundamental performance limitations. Indeed, reducing the interaction between layers can be practically achieved, by judicious optimization of the compensated synthetic antiferromagnetic reference layer as well as by minimizing the interfacial roughness of the CoFeB/MgO/Co₂FeSi trilayer complex to reduce roughness-induced magnetic coupling.

4. Conclusion

Magnetization reversal of the Co₂FeSi layer of an unpatterned, bottom-pinned MTJ film with 149% TMR has been observed using the MOIF technique. The synthetic antiferromagnetic reference layer exerts a significant influence on the reversal behavior of the free layer, resulting in coherent rotation of the Co₂FeSi layer under in-plane fields applied perpendicular to the in-plane exchange bias axis of the reference layer. This behavior should be considered alongside engineering shape anisotropy to realize a strong linear response of the free layer for magnetic field sensing applications. Fields applied collinear with the exchange biasing direction result in asymmetric domain wall propagation behavior relative to the reference layer magnetization direction, which are likely to factor heavily in the reversal behavior of patterned elements, whose magnetostatic coupling may significantly exceed their magnitudes in a continuous film.

5. Acknowledgements

PP would like to acknowledge the support from the Seed Funding Program for Basic Research, Seed Funding Program for Applied Research, and Small Project Funding Program from The University of Hong Kong, and the support from the Research Grants Council-General Research

Fund (RGC-GRF) under Grant HKU 17204617. This work was partially supported by the National Institute of Standards and Technology.

References

- [1] S. Tsunegi, Y. Sakuraba, M. Oogane, K. Takanashi, and Y. Ando, "Large tunnel magnetoresistance in magnetic tunnel junctions using a Co₂MnSi Heusler alloy electrode and a MgO barrier," *Applied Physics Letters*, vol. 93, no. 11, p. 112506, 2008/09/15 2008.
- [2] E. Ozawa, S. Tsunegi, M. Oogane, H. Naganuma, and Y. Ando, "The effect of inserting thin Co₂MnAl layer into the Co₂MnSi/MgO interface on tunnel magnetoresistance effect," *Journal of Physics: Conference Series*, vol. 266, p. 012104, 2011/01/01 2011.
- [3] W. Wang *et al.*, "Coherent tunneling and giant tunneling magnetoresistance in $\text{Co}_2\text{FeAl}/\text{MgO}/\text{CoFe}$ magnetic tunneling junctions," *Physical Review B*, vol. 81, no. 14, p. 140402, 04/13/ 2010.
- [4] N. Tezuka, N. Ikeda, F. Mitsuhashi, and S. Sugimoto, "Improved tunnel magnetoresistance of magnetic tunnel junctions with Heusler Co₂FeAl_{0.5}Si_{0.5} electrodes fabricated by molecular beam epitaxy," *Applied Physics Letters*, vol. 94, no. 16, p. 162504, 2009/04/20 2009.
- [5] S. Wurmehl, G. H. Fecher, H. C. Kandpal, V. Ksenofontov, C. Felser, and H. J. Lin, "Investigation of Co₂FeSi: The Heusler compound with highest Curie temperature and magnetic moment," *Applied Physics Letters*, vol. 88, no. 3, Jan 16 2006, Art. no. 032503.
- [6] S. Trudel, O. Gaier, J. Hamrle, and B. Hillebrands, "Magnetic anisotropy, exchange and damping in cobalt-based full-Heusler compounds: an experimental review," *Journal of Physics D-Applied Physics*, vol. 43, no. 19, May 2010, Art. no. 193001.
- [7] J. Hamrle *et al.*, "Huge quadratic magneto-optical Kerr effect and magnetization reversal in the Co₂FeSi Heusler compound," *Journal of Physics D-Applied Physics*, vol. 40, no. 6, pp. 1563-1569, Mar 2007.
- [8] A. Gloskovskii *et al.*, "A spatially resolved investigation of the local, micro-magnetic domain structure of single and polycrystalline Co₂FeSi," *Journal of Physics D-Applied Physics*, vol. 40, no. 6, pp. 1570-1575, Mar 2007.
- [9] P. J. Chen, G. Feng, and R. D. Shull, "Use of Half Metallic Heusler Alloys in CoFeB/MgO/Heusler Alloy Tunnel Junctions," *IEEE Transactions on Magnetics*, vol. 49, no. 7, pp. 4379-4382, Jul 2013.
- [10] D. C. Worledge and P. L. Trouilloud, "Magnetoresistance measurement of unpatterned magnetic tunnel junction wafers by current-in-plane tunneling," *Applied Physics Letters*, vol. 83, no. 1, pp. 84-86, 2003/07/07 2003.
- [11] L. H. Bennett *et al.*, "Magneto- optical indicator film observation of domain structure in magnetic multilayers," *Applied Physics Letters*, vol. 66, no. 7, pp. 888-890, 1995/02/13 1995.
- [12] L. A. Dorosinskii, M. V. Indenbom, V. I. Nikitenko, Y. A. Ossip'yan, A. A. Polyanskii, and V. K. Vlasko-Vlasov, "Studies of HTSC crystal magnetization features using indicator magneto optic films with in-plane anisotropy," *Physica C: Superconductivity*, vol. 203, no. 1, pp. 149-156, 1992/12/01/ 1992.
- [13] D. B. Gopman, Y. P. Kabanov, J. Cui, C. S. Lynch, and R. D. Shull, "Influence of internal geometry on magnetization reversal in asymmetric permalloy rings," *Applied Physics Letters*, vol. 109, no. 8, Aug 2016, Art. no. 082407.
- [14] M. Staruch *et al.*, "Magnetoelastic Effects in Doubly Clamped Electroplated Co₇₇Fe₂₃ Microbeam Resonators," *Physical Review Applied*, vol. 11, no. 3, Mar 2019, Art. no. 034028.

- [15] M. Staruch *et al.*, "Reversible strain control of magnetic anisotropy in magnetoelectric heterostructures at room temperature," *Scientific Reports*, vol. 6, Nov 2016, Art. no. 37429.
- [16] V. S. Gornakov *et al.*, "Experimental study of the microscopic mechanisms of magnetization reversal in FeNi/FeMn exchange-biased ferromagnet/antiferromagnet polycrystalline bilayers using the magneto-optical indicator film technique," *Physical Review B*, vol. 73, no. 18, p. 184428, 05/22/ 2006.
- [17] V. I. Nikitenko *et al.*, "Asymmetry of domain nucleation and enhanced coercivity in exchange-biased epitaxial NiO/NiFe bilayers," *Physical Review B*, vol. 57, no. 14, pp. R8111-R8114, 04/01/ 1998.
- [18] V. I. Nikitenko *et al.*, "Asymmetry in Elementary Events of Magnetization Reversal in a Ferromagnetic/Antiferromagnetic Bilayer," *Physical Review Letters*, vol. 84, no. 4, pp. 765-768, 01/24/ 2000.
- [19] T. R. Gao *et al.*, "Hysteretic Behavior of Angular Dependence of Exchange Bias in FeNi/FeMn Bilayers," *Physical Review Letters*, vol. 99, no. 5, p. 057201, 07/30/ 2007.
- [20] W. Skowroński *et al.*, "Interlayer exchange coupling and current induced magnetization switching in magnetic tunnel junctions with MgO wedge barrier," vol. 107, no. 9, p. 093917, 2010.
- [21] F. A. Shah, V. K. Sankar, P. Li, G. Csaba, E. Chen, and G. H. Bernstein, "Compensation of orange-peel coupling effect in magnetic tunnel junction free layer via shape engineering for nanomagnet logic applications," vol. 115, no. 17, p. 17B902, 2014.
- [22] M. Gottwald *et al.*, "Asymmetric magnetization reversal in dipolarly coupled spin valve structures with perpendicular magnetic anisotropy," *Physical Review B*, vol. 85, no. 6, p. 064403, 02/03/ 2012.
- [23] D. B. Gopman *et al.*, "Asymmetric switching behavior in perpendicularly magnetized spin-valve nanopillars due to the polarizer dipole field," *Applied Physics Letters*, vol. 100, no. 6, p. 062404, 2012/02/06 2012.

Figures and Captions

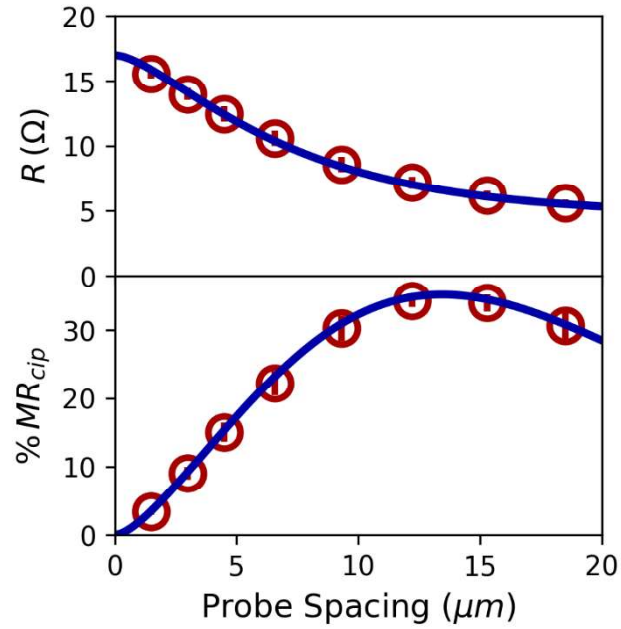


Figure 1: (Top) Sheet resistance of the MTJ versus probe spacing in the parallel state (red circles). (Bottom) CIPT tunneling magnetoresistance (red circles) versus probe spacing. Error bars reflect one-sigma uncertainty in measured resistance values. Blue solid lines reflect solution to CIPT model with $TMR = 149\%$ and $RA=1100 \Omega \cdot \mu\text{m}^2$.

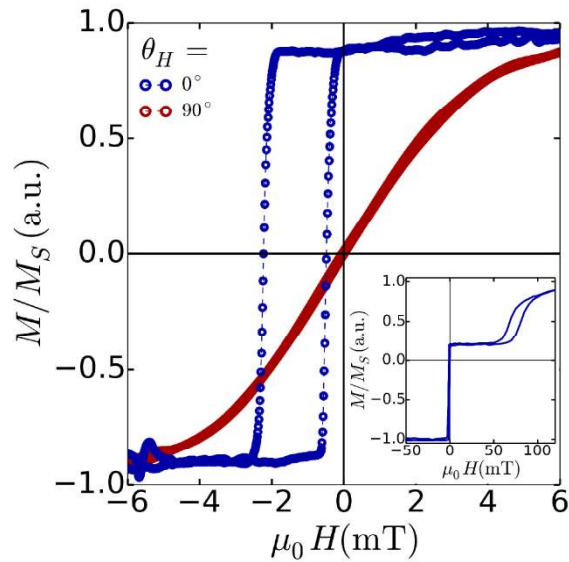


Figure 2: Magnetic hysteresis loop with in-plane applied field along the horizontal (0°) exchange bias axis and at 90° to the exchange bias showing reversal of the free layer. Inset: magnetic hysteresis loop with applied field along the exchange bias axis showing reversal of the free layer and the reference layer.

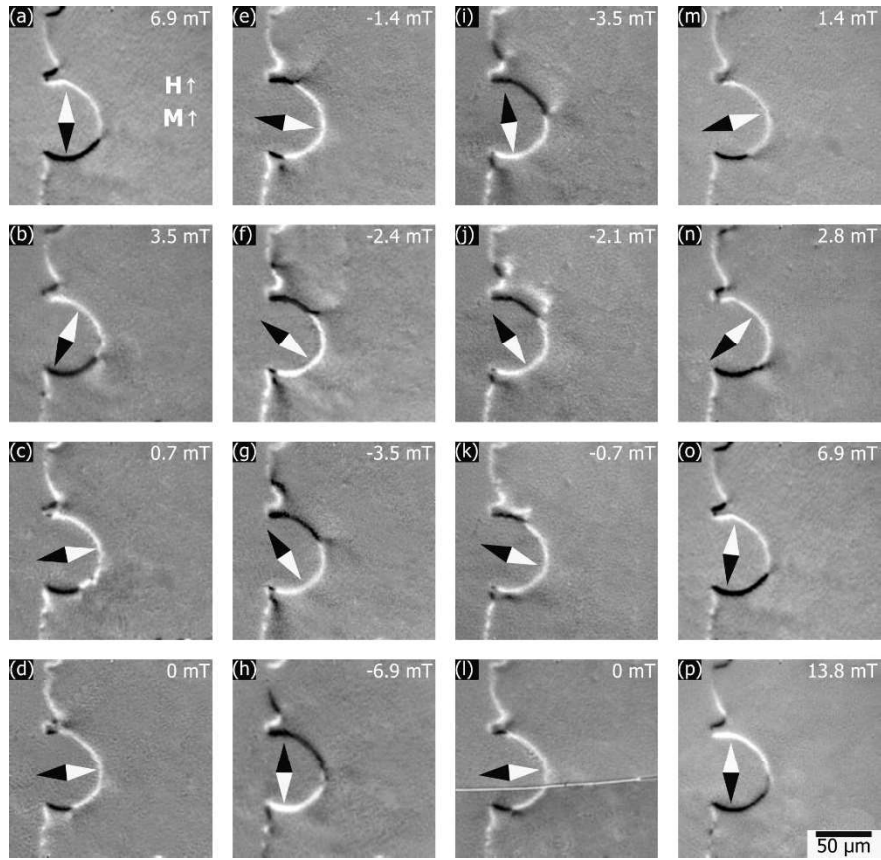


Figure 3: MOIF images for H applied perpendicular to the exchange bias direction: (a)-(h) are for $\mu_0 H$ sequentially decreased from 6.9 mT to -6.9 mT, and (i)-(p) are for $\mu_0 H$ sequentially increased from -3.5 mT to 13.8 mT, respectively.

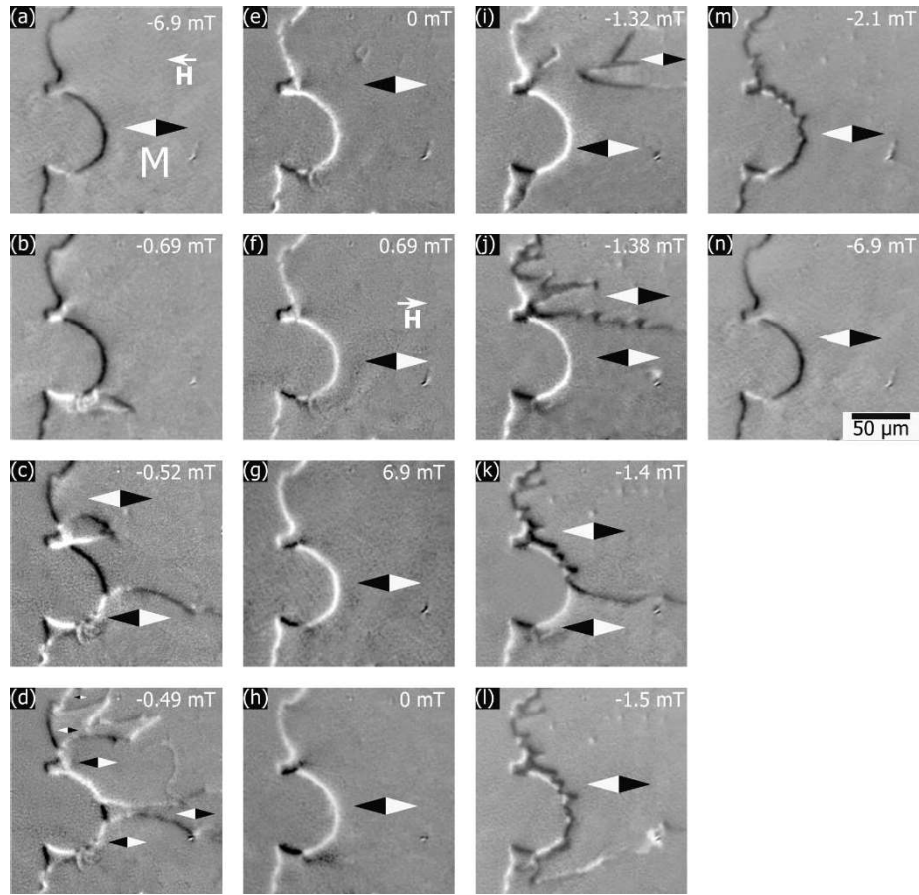


Figure 4: MOIF images for H applied parallel to the exchange bias direction: (a)-(g) are for $\mu_0 H$ sequentially increased from -6.9 mT to 6.9 mT, and (h)-(n) are for $\mu_0 H$ sequentially decreased from 0.0 mT to -6.9 mT, respectively.